



Stiffness Modeling of a Stewart-Platform-Based Milling Machine

Charles Clinton

Research Associate

University of Maryland
Department of Mechanical Engineering and
Institute for Systems Research
College Park, Maryland 20742
and
Machine Systems
Intelligent Systems Division

Guangming Zhang

University of Maryland
Department of Mechanical Engineering and
Institute for Systems Research
College Park, Maryland 20742

Albert J. Wavering

Machine Systems
Intelligent Systems Division

U.S. DEPARTMENT OF COMMERCE
Technology Administration
National Institute of Standards
and Technology
Bldg. 220 Rm. B124
Gaithersburg, MD 20899

QC
100
.U56
NO.5918
1996

NIST

Stiffness Modeling of a Stewart-Platform-Based Milling Machine

Charles Clinton

Research Associate

University of Maryland
Department of Mechanical Engineering and
Institute for Systems Research
College Park, Maryland 20742
and
Machine Systems
Intelligent Systems Division

Guangming Zhang

University of Maryland
Department of Mechanical Engineering and
Institute for Systems Research
College Park, Maryland 20742

Albert J. Wavering

Machine Systems
Intelligent Systems Division

U.S. DEPARTMENT OF COMMERCE
Technology Administration
National Institute of Standards
and Technology
Bldg. 220 Rm. B124
Gaithersburg, MD 20899

October 1996



U.S. DEPARTMENT OF COMMERCE
Michael Kantor, Secretary

TECHNOLOGY ADMINISTRATION
Mary L. Good, Under Secretary for Technology

NATIONAL INSTITUTE OF STANDARDS
AND TECHNOLOGY
Arati Prabhakar, Director

Stiffness Modeling of a Stewart-Platform-Based Milling Machine

Charles M. Clinton and Guangming Zhang
Department of Mechanical Engineering & Institute for Systems Research
University of Maryland, College Park, MD 20742

Albert J. Wavering
Intelligent Systems Division
National Institute of Standards and Technology
Gaithersburg, MD, 20899

Abstract

This paper presents the development of a mathematical model describing the stiffness of a Stewart-platform-based milling machine. Matrix structural analysis is used to derive the stiffness matrix for each of the elements in the model and assemble them into a system-wide stiffness matrix. By incorporating the inverse kinematics of the machine tool, the system model is used to visualize the stiffness variation over the mill's workspace. Estimation of the system parameters is conducted through experimental stiffness measurements. Computer simulation is used to demonstrate how the developed stiffness model suggests an optimization process for tool-path planning.

1. Introduction

Competitive pressures compel machine tool designers to continually search for equipment that can deliver higher accuracies and material removal rates. The search for new and innovative machine tool designs has led to an exploration of the capabilities of parallel mechanisms. Typically, these mechanisms consist of a moveable platform connected to a rigid base through multiple, identically jointed and extensible struts. The unique characteristics of high stiffness and high speed, combined with versatile contouring capabilities have made parallel mechanisms good potential candidates for the machine tool industry to advance machining performance.

The potential use of parallel mechanisms as machine tools dates back to Stewart's paper on a six-degree of freedom mechanism [1]. He designed this mechanism, commonly called a Stewart platform, to provide motion for a flight simulator, but also suggested its use as a machine tool. It has not been until recently, though, that computing power and control software have matured to the level necessary for the development of commercial parallel machine tools. Several prototypes of Stewart platform based machine tools are now being tested throughout the world.

In this paper, a stiffness model of a Stewart platform based milling machine is presented. This

model uses traditional matrix structural analysis in conjunction with preliminary experimental stiffness results from the Ingersoll Octahedral-Hexapod located at the National Institute of Standards and Technology (NIST). The use of matrix structural analysis differs from the traditional approach to robotic stiffness modeling taken by Gosselin[2], which relies on the calculation of a Stewart platform's Jacobian.

The objective of this stiffness model is to provide an understanding of how the stiffness of the machine tool changes as a function of its workspace. This can be accomplished using a mapping algorithm. It can also be combined with numerical control programs to examine stiffness variation as the machine follows a tool path. It should be pointed out that the work presented in this paper demonstrates the importance of using the system stiffness model to maximize the machine's stiffness during operation.

2. Ingersoll Octahedral-Hexapod

The NIST Ingersoll Octahedral-Hexapod¹ is a prototype Stewart platform based milling

¹ Certain commercial equipment, instruments, or materials are identified in this paper to specify the experimental procedure adequately. Such identification is not intended to imply recommendation or endorsement by the National Institute of Standards and Technology, nor is it intended to imply that the

machine. As illustrated in Figure 1, the machine tool consists of a small platform that supports the spindle motor and tool connected to a space frame structure through six identical struts. These struts consist of two spherical joints connected by a servo driven ball screw. The spindle platform is translated and rotated by changing the length of the ball screw in each strut.

The use of six struts imparts six degrees of freedom to the milling machine. This allows the Hexapod to machine complex contoured surfaces common in areas such as tool and die manufacturing and the aerospace industry. The unique geometry of the Hexapod means that machining forces are primarily distributed as axial loads throughout the structure, greatly increasing stiffness. This also provides for the use of lighter components, allowing higher feed rates and reduces the need for heavy duty foundations necessary for traditional machine tools.

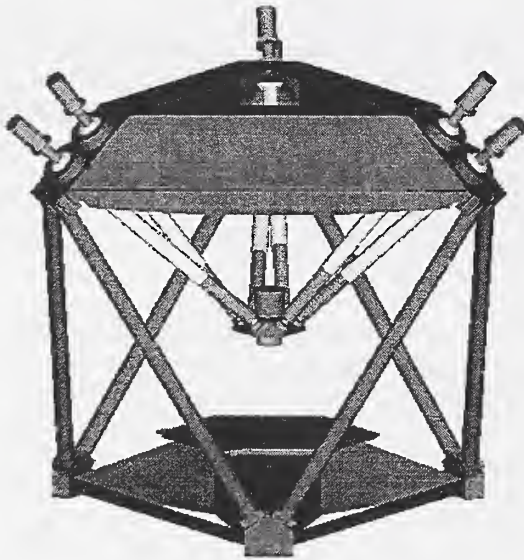


Figure 1. NIST Ingersoll Octahedral Hexapod

3. Development of Stiffness Model

The Hexapod stiffness model is based on matrix structural analysis[3], which models structures as a combination of elements and nodes. Equation 1 describes the basic relationship in this method of analysis, where $\{F\}$ is a force vector

applied to the nodes of the structure and $\{x\}$ is the displacement of the nodes due to those applied forces. $[k]$ is the structure stiffness matrix that relates the two vectors. The stiffness matrix depends on the nature of the elements in the structure, whether they are truss or frame elements, their geometric orientation and connectivity.

$$\{F\} = [k] \cdot \{x\} \quad (1)$$

In this study, the Hexapod stiffness model relies on truss elements. These elements consist of two nodes and are only capable of linear deformation along their length, as assumed. The deflection of a truss element in its local coordinate frame is thus described by equation 2, where i and j represent the two nodes of the element and $[F]$ and $[u]$ are the external forces and nodal displacements respectively. The element is assumed to lie along the local x axis. This matrix is scaled by the cross-sectional area of the element, A , the elastic modulus, E , and the length of the element L .

$$\begin{bmatrix} F_{ix} \\ F_{iy} \\ F_{iz} \\ F_{jx} \\ F_{jy} \\ F_{jz} \end{bmatrix} = \frac{AE}{L} \begin{bmatrix} 1 & 0 & 0 & -1 & 0 & 0 \\ 0 & 0 & 0 & 0 & 0 & 0 \\ 0 & 0 & 0 & 0 & 0 & 0 \\ -1 & 0 & 0 & 1 & 0 & 0 \\ 0 & 0 & 0 & 0 & 0 & 0 \\ 0 & 0 & 0 & 0 & 0 & 0 \end{bmatrix} \begin{bmatrix} u_{ix} \\ u_{iy} \\ u_{iz} \\ u_{jx} \\ u_{jy} \\ u_{jz} \end{bmatrix} \quad (2)$$

When analyzing a structure, it is necessary to transform the element stiffness matrices in the local coordinate system to the global coordinate system of the structure. This is accomplished through the use of a rotation matrix (eq. 3), where i_u , j_v , and k_w are the unit vectors in the local coordinate system and i_x , j_y , and k_z are the unit vectors in the global coordinate system.

$$R = \begin{bmatrix} i_x \cdot i_u & i_x \cdot j_v & i_x \cdot k_w \\ j_y \cdot i_u & j_y \cdot j_v & j_y \cdot k_w \\ k_z \cdot i_u & k_z \cdot j_v & k_z \cdot k_w \end{bmatrix} \quad (3)$$

Letting $c_1 = \frac{X_2 - X_1}{L}$, $c_2 = \frac{Y_2 - Y_1}{L}$, and $c_3 = \frac{Z_2 - Z_1}{L}$, where X_1 , X_2 , etc. represent the x , y , or z global coordinates of the two nodes associated with each truss element and

materials or equipment identified are necessarily the best available for the purpose.

$L = \sqrt{(X_2 - X_1)^2 + (Y_2 - Y_1)^2 + (Z_2 - Z_1)^2}$, it can then be shown that the overall stiffness matrix for one truss element in global coordinates is equal to equation 4 [3].

$$[k] = \frac{AE}{L} \begin{bmatrix} c_1^2 & c_1c_2 & c_1c_3 & -c_1^2 & -c_1c_2 & -c_1c_3 \\ c_2c_1 & c_2^2 & c_2c_3 & -c_2c_1 & -c_2^2 & -c_2c_3 \\ c_3c_1 & c_3c_2 & c_3^2 & -c_3c_1 & -c_3c_2 & -c_3^2 \\ -c_1^2 & -c_1c_2 & -c_1c_3 & c_1^2 & c_1c_2 & c_1c_3 \\ -c_2c_1 & c_2^2 & -c_2c_3 & c_2c_1 & c_2^2 & c_2c_3 \\ -c_3c_1 & -c_3c_2 & -c_3^2 & c_3c_1 & c_3c_2 & c_3^2 \end{bmatrix} \quad (4)$$

This equation is combined with other element stiffness matrices to create a single stiffness matrix for the entire structure. This is accomplished by adding the individual stiffness matrices together with respect to the connectivity of the elements in the overall structure.

In this study, twenty-five elements are used to represent the Ingersoll Octahedral-Hexapod. Figure 2 a, b shows the location of those elements in the machine tool model. Truss elements are assumed to be pin jointed at each end and unable to transmit a moment from one element to the next. Due to this, it is necessary to use a large number of truss elements to represent the spindle platform to ensure that the spindle platform elements form a locked kinematic structure. Furthermore, the tool element is included to properly transmit the moment experienced by the machine due to lateral forces on the tool.

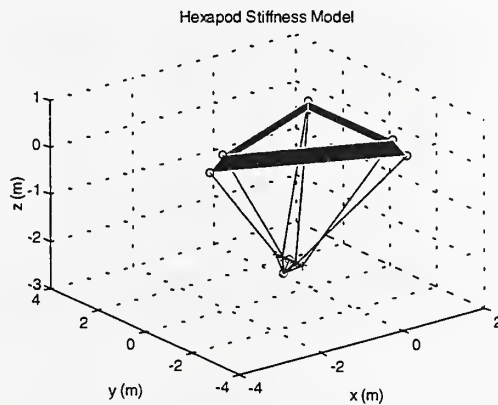


**Figure 2a. Machine Position (-0.3 m,0.3m,0.3m)
Machine Orientation (-30,0,0) (degrees)**

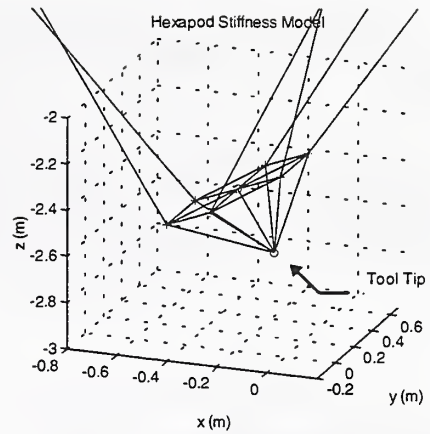


Figure 2b. Detail of Spindle Elements

The second assumption made in this analysis is that the majority of the mill's deflection under load occurs in the struts of the machine instead of the spindle platform. This is implemented by assigning a high stiffness to the elements representing the spindle platform. Figure 3 depicts the error between the modeled stiffness and experimental measurements, averaged over all experimental data points and stiffness measurement directions, for varying stiffnesses of the spindle platform elements. As seen in Figure 3, assigning stiffnesses above 1×10^{10} N/m to the spindle platform elements minimizes the average error between simulated stiffness and measured stiffness.

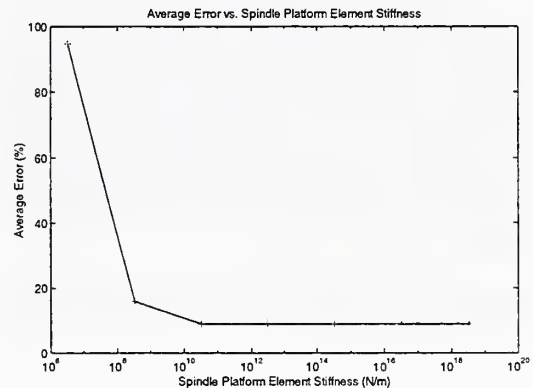


Figure 3. Plot of Simulation Error Versus Spindle Platform Element Stiffness

It should be noted that the compliance of the spindle bearings and tool are not addressed in this model. This is because these compliances were not measured by the experimental set-up described later in this paper.

The displacement of the structure due to a load on the tool is solved using Gaussian elimination.

Stiffness is then calculated for a machine pose and force vector by equation 5, where F is the scalar load applied to the tool tip and x is the tool tip's deflection in the same direction as the applied force.

$$k = \frac{F}{x} \quad (5)$$

3.1 Strut Stiffness Model

In this simulation, the struts of the Hexapod are assumed to change stiffness as a linear function of length. This function is developed with the aid of experimental results, using the concept of average error. To calculate the average error, the Hexapod stiffness model is iterated over all experimental data points and the amount of error between modeled and experimentally determined stiffness is calculated for each of the three directions of measurement, x , y , and z . The objective then is to define a linear model of strut stiffness which produces the least average error. A total of forty-two stiffness measurements are used in determining the strut stiffness model.

In the development of the strut stiffness model, two independent parameters are identified. These are the stiffnesses, k_{L1} and k_{L2} , at two arbitrarily chosen strut lengths, L_1 and L_2 . The dependent parameter in this case is the average error between the modeled stiffness and the experimental results. To minimize the average error, the independent variables are optimized using a univariate search routine.

The resulting stiffness model used in this simulation is given by equation 6.

$$k = \frac{k_{L1} - k_{L2}}{L_1 - L_2} \cdot (L_{strut} - L_2) + k_{L2} \quad (6)$$

The optimization resulted in the values of 46.5×10^6 N/m and 32.5×10^6 N/m for k_{L1} and k_{L2} in order to minimize the average error, values of which are presented later in this paper. L_1 and L_2 are equal to 2.5616 m and 3.2132 m respectively. These values correspond to the strut lengths

necessary to reach the two planes in the Hexapod's workspace where stiffness measurements were made.

Expanded stiffness measurement coverage of the workspace, especially in a greater variety of x - y planes, would allow the investigation of the nonlinear stiffness aspects of the ball screws.

3.2 Inverse Kinematics

According to the derived strut stiffness equation (eq. 6), the stiffness of a strut depends on its length. Therefore, it is necessary to calculate the inverse kinematics of the Hexapod to determine the strut lengths for any given machine position and orientation. Unlike many serial mechanisms, the calculation of the inverse kinematics of a parallel mechanism is generally straight-forward [4].

The first step in the inverse kinematics problem is to assign coordinate systems to the fixed and moving reference frames [5],[6]. These correspond to the top center of the base structure and the center of the spindle platform. Furthermore, reference points are used to geometrically define the spindle platform. These points are coincident with the center of the spherical joints which connect the spindle platform to the struts. Additional points are located at the tool tip and at the intersection of the tool with the plane of the spherical joints. These points are used as references for the later assembly of elements into a machine model.

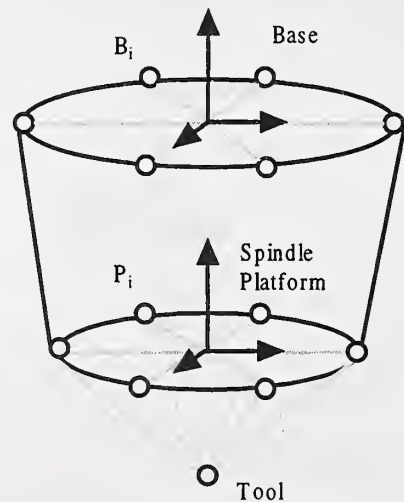


Figure 4. Base and Platform Coordinate Systems

In general spatial motion, a moving system, in this case the spindle platform, is displaced and rotated from its initial position to a new location in space. For each solution of the inverse kinematics, we assume that the spindle platform's coordinate frame is initially coincident with the base coordinate frame. The resulting translation to the spindle platform's current location can then be described by a single three-term vector, q , containing cartesian coordinates. The rotation of the machine can also be described by three angular variables, roll, pitch, and yaw.

(q_x, q_y, q_z) -Coordinates of the center of the spindle platform with respect to the base frame

α (roll angle)-Rotation about the x axis of the base frame

β (pitch angle)-Rotation about the y axis of the base frame

γ (yaw angle)-Rotation about the z axis of the base frame

The spindle platform is first rotated and the location of the spherical joints are described in the base coordinate frame by equation 7,

$$\text{Rotated } P_i = R_{\alpha\beta\gamma} \text{ Platform } P_i \quad (7)$$

where the rotation matrix is defined as:

$$R_{\alpha\beta\gamma} = \begin{bmatrix} \cos\alpha \cos\beta & \cos\alpha \sin\beta \cos\gamma - \sin\alpha \cos\gamma & \cos\alpha \sin\beta \cos\gamma + \sin\alpha \sin\gamma \\ \sin\alpha \cos\beta & \sin\alpha \sin\beta \sin\gamma - \cos\alpha \cos\gamma & \sin\alpha \sin\beta \cos\gamma - \cos\alpha \sin\gamma \\ -\sin\beta & \cos\beta \sin\gamma & \cos\beta \cos\gamma \end{bmatrix} \quad (8)$$

These points are then translated using the transformation vector, q , as illustrated in Figure 5.

This relation is given by:

$$\text{Base } P_i = \text{Rotated } P_i + q_{xyz} \quad (9)$$

Overall, this transformation can be represented by the following equation:

$$\text{Base } P_{xyz} = R_{\alpha\beta\gamma} \text{ Platform } P_{uvw} + q_{xyz} \quad (10)$$

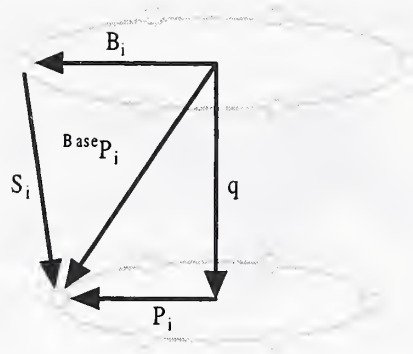


Figure 5. Inverse Kinematic Vectors

Vectors representing the struts can then be calculated,

$$S_i = \text{Base } P_i - B_i \quad (11)$$

where B_i is the vector, defined in the base frame, from the base coordinate system to the connection of the strut with the base. The length of the leg, L_i , is then the magnitude of the strut vector, S_i .

$$L_i = |S_i| \quad (12)$$

4. Experimental Stiffness Measurements

In this research, stiffness measurements were made on the NIST Ingersoll Octahedral-Hexapod to validate the system stiffness model. A relatively high degree of uncertainty exists in this data due to the observed stiffness variation between data points and the variation between subsequent measurements at the same data point. The data are presented with the understanding that these are preliminary results subject to further refinement with improved experimental techniques. They are of sufficient quality, though, to validate the approach taken to the modeling of the NIST Ingersoll Hexapod's stiffness characteristics.

4.1 Methodology

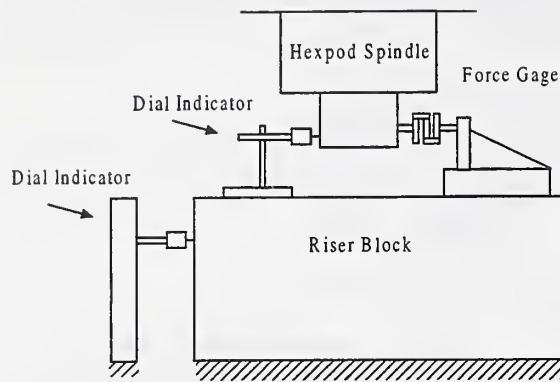


Figure 6. Experimental Set-up for $z = 1268.225$ mm

The experimental procedure was similar to the stiffness tests outlined in the ASME standard B5.54[7]. The machine was restrained from movement in the x, y, or z direction with a force gauge, while the machine was jogged in 100 μm increments (fig. 6). The actual displacement of the machine was recorded by digital dial indicators. For each measurement position, the machine was jogged from zero to +200 μm , from +200 μm to -200 μm , and from -200 μm back to zero. Force and displacement data were recorded for each movement increment.

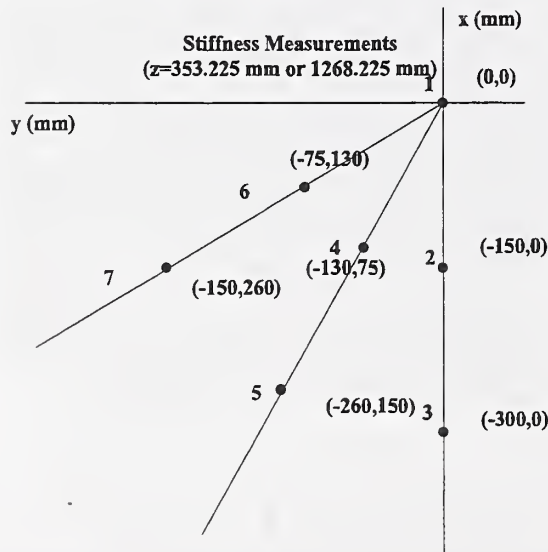


Figure 7. Location of Stiffness Measurements in Work Plane

Selection of measurement position in the machine's workspace took into account the

machine's symmetry. Stiffness was measured at discrete points within a 30° planar wedge of the workspace at two different z heights (Fig. 7). Measurement positions were selected along a radius leading to a strut-structure attachment and halfway in between two leg sets. This would allow the measurement of the stiffness gradient in the radial and circumferential directions.

4.2 Analysis and Sample Calculations

At each data point, measurements were made in the x, y, and z directions. Only data recorded when the machine was at the ± 200 μm displacement extremes is used in the calculation of the stiffness. This is done to reduce the error in our calculations by attempting to eliminate the machine's backlash from our measurements, in accordance with ASME standard B5.54. Equation 13 is used for the stiffness calculations, where F is the measured force in Newtons and D is the measured deflection of the machine tool in millimeters.

$$k = \frac{F_{y=0.2} - F_{y=-0.2}}{0.4\text{mm} - (D_{y=0.2} - D_{y=-0.2})} \quad (13)$$

4.3 Data Summary

Table 1 lists the measured stiffness data collected for each position in two different planes of the machine's workspace. The position values given in Table 1 indicated the programmed nominal positions used for these tests.

Table 1. Experimental and Modeled Stiffness

Data Summary for z elevation of 1268.225 mm									
Position (mm)			Machine Stiffness (N/mm)			Stiffness Model (N/mm)			
X	Y	Z	X	Y	Z	X	Y	Z	
0	0	1268.23	56813	64522	85714	57950	57950	110141	
-150	0	1268.23	62636	53544	88617	59959	55210	107719	
-300	0	1268.23	60100	48908	97001	60963	51978	100372	
-130	75	1268.23	66123	55236	93922	59544	55560	107723	
-260	150	1268.23	71105	74527	103778	60061	52614	100413	
-75	130	1268.23	62062	67234	103065	58646	56371	107970	
-150	260	1268.23	58257	67397	104348	58404	53998	102172	
			Std. Dev	Std. Dev	Std. Dev	Std. Dev	Std. Dev	Std. Dev	
			4890	9197	7560	1070	2103	4087	
Data Summary for z elevation of 353.225 mm									
Position (mm)			Machine Stiffness (N/mm)			Stiffness Model (N/mm)			
X	Y	Z	X	Y	Z	X	Y	Z	
0	0	353.225	32186	33656	121235	37527	37527	119346	
-150	0	353.225	51989	32281	105608	39380	35114	116404	
-300	0	353.225	47356	32502	127158	40670	32232	107722	
-130	75	353.225	34132	35218	104916	38961	35446	116449	
-260	150	353.225	42238	30814	113975	39635	32864	108043	
-75	130	353.225	40578	31387	99206	38038	36236	116663	
-150	260	353.225	41503	34093	104472	37584	34342	109560	
			Std. Dev	Std. Dev	Std. Dev	Std. Dev	Std. Dev	Std. Dev	
			6913	1556	10185	1171	1851	4830	

The stiffness measurements made on the Hexapod exhibit a high degree of variability. This occurred between both geometrically close

measurement positions and consecutive measurements at the same measurement position. Standard deviations in the above data can be as high as 10,185 N/mm. In an effort to isolate the source of much of the variation, three measurements were made at point 1 with loading in the y direction. Without unclamping the structure between measurements, the standard deviation was 44 N/mm. If the experimental set-up was unclamped, re-clamped, and the force gage re-zeroed, the standard deviation over three measurements was 244 N/mm. In a separate test of two measurements where loading was in the x direction, the standard deviation was 1442 N/mm. Future refinements in experimental procedure will be necessary to increase the accuracy of these measurements.

Data listed in Table 1 shows the model predicted stiffness for the corresponding data points. The average difference between model and experimental results for the $z = 1268.225$ mm plane is equal to 9.05%. Average difference for the $z = 353.225$ mm plane is equal to 8.95%.

5. Stiffness Mapping

The complex geometry of the Hexapod milling machine means that the identification of maximum and minimum regions of stiffness in the workspace is not an intuitive process. Stiffness maps, therefore, can aid in workpiece placement to maximize machine stiffness and thereby increase part accuracy. Figure 8 shows the stiffness of the Hexapod over a constant z height of 1.2 m. The computer model was posed, without rotation of the spindle platform, over a 0.3 m by 0.3 m workspace. The stiffness was then calculated by applying a planar force vector in the direction from the current position of the spindle to the center of the workspace. The purpose of this force application was to match the applied force to the machine's radial geometrical symmetry. This symmetry is reflected in the stiffness map with three stiffness maxima and three minima. These maxima correspond to the struts' intersection with the base space frame. Figure 9 illustrates the change in z -direction stiffness over a planar workspace.

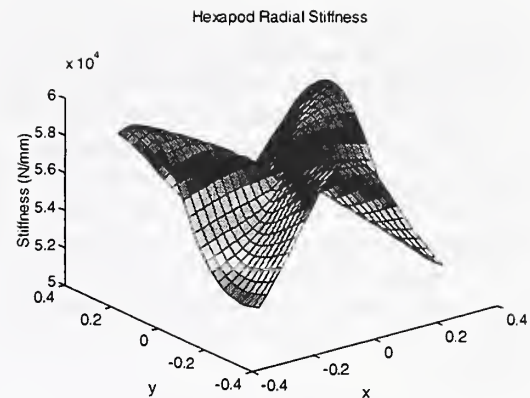


Figure 8. Stiffness of Hexapod Under Load Vector from (x,y) to (0,0) at $z = 1.2$ m

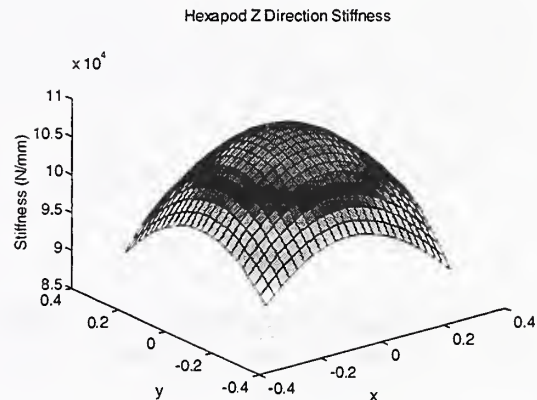


Figure 9. Stiffness of Hexapod in Z Direction at $z = 1.2$ m

6. Tool Path Planning

An application of the system stiffness model is tool-path planning. The complexity of the stiffness variation through the workspace suggests that identical tool paths in several areas of the workspace can be compared to maximize the machine's stiffness and minimize the variation in stiffness over a tool path. Both of these objectives are advantageous to the machining of high accuracy parts.

A case study is presented in which a simulated tool path is run in four different areas of the workspace. Figure 10 shows the location of these four areas. Stiffness is calculated along the path, by simulating a load on the machine tangential to the machine's movement. The Hexapod's spindle

remains vertical throughout the machine's travel. Discontinuities in the stiffness plots exist due to this load changing direction. Results detailed in Figs. 11, 12, and 13 show that the overall stiffness of the path increases as the z height of the movement plane increases. An increase in overall stiffness is somewhat offset by an increase in the variation of the stiffness over the tool path. Simulations at the same z height at different positions and orientations on the work-plane show stiffnesses of the same magnitude, with a small difference in standard deviation.

Location of Tool Paths in Workspace

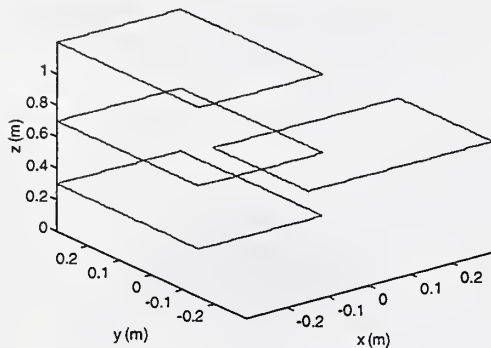


Figure 10. Location in the Hexapod Workspace of the Four Test Tool Paths

Stiffness vs. Planar Machine Path

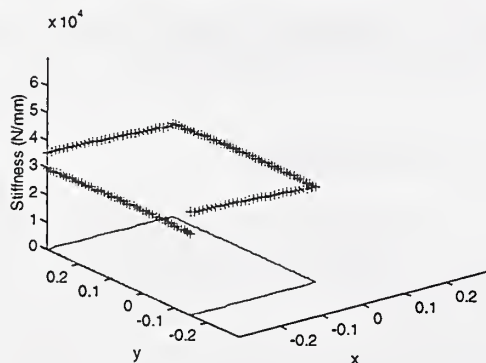


Figure 11. Tool Path at $z = 0.3$ m. Average Stiffness = 33,828 N/mm Range = 8,377 N/mm

Stiffness vs. Planar Machine Path

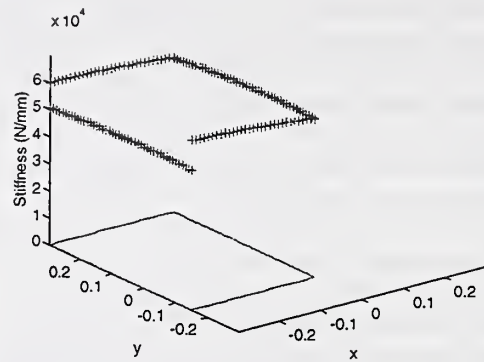


Figure 12. Tool Path at $z = 1.2$ m. Average Stiffness of 57,192 N/mm Range = 12,075 N/mm

Stiffness vs. Planar Machine Path

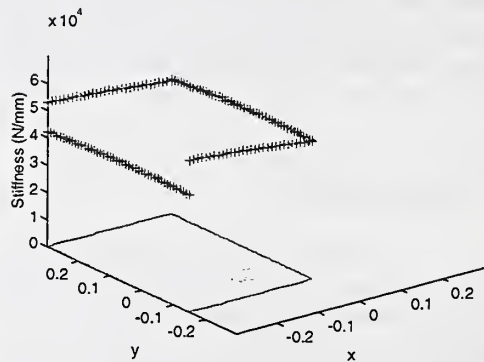


Figure 13. Tool Path at $z = 0.7$ m. Average Stiffness of 49,201 N/mm Range = 13,771 N/mm

Stiffness vs. Planar Machine Path

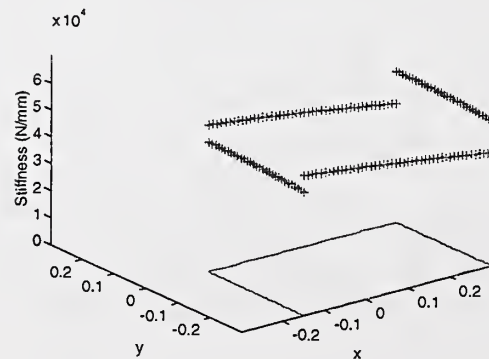


Figure 14. Tool Path at $z = 0.7$ m. Average Stiffness of 49,441 N/mm Range = 14,195 N/mm

7. Conclusions

1. The preliminary stiffness results from the Ingersoll Octahedral-Hexapod support the validity of this approach to stiffness modeling.
2. Stiffness as a function of the workspace is complex and varies considerably due to the machine's position and orientation, as well as the orientation of the applied structural load.
3. Tool-path stiffness increases as the height of the tool path increases and for the case study was mostly independent of its location in a particular x-y plane of the workspace. The latter statement may not be true over more complex tool paths involving non-orthogonal cuts.

8. Acknowledgments

The authors would like to thank Mr. Fred Rudder of the National Institute of Standards and Technology for his support of this work. Special thanks go to Dr. Joe Drescher of United Technologies, Pratt & Whitney, Inc. for his contribution of time and equipment to this research.

9. References

- [1] Stewart, D., 1965, "A Platform with Six Degrees of Freedom", Proc. Inst. of Mech. Engr., London, England, Vol. 180, pp. 371-386
- [2] Gosselin, C., 1990, "Stiffness Mapping for Parallel Manipulators", Transactions on Robotics and Automation, Vol. 6, No. 3
- [3] Armenakas, A. E., 1991, *Modern Structural Analysis: the Matrix Method Approach*, McGraw-Hill, Inc., New York
- [4] Tsai, L.W., *ENME603: Advanced Mechanisms and Robot Manipulators*, Class Notes, University of Maryland-Institute for Systems Research
- [5] Wang, J., 1992, "Workspace Evaluation and Kinematic Calibration of Stewart Platforms", Ph.D. Dissertation, Florida Atlantic University
- [6] Fichter, E. F., 1986, A Stewart Platform Based Manipulator: General Theory and Practical Construction," International Journal of Robotics Research, Vol. 5, pp. 157-182
- [7] ANSI/ASME B5.54-1992, "Methods for Performance Evaluation of Computer Controlled Machining Centers", ASME, New York, 1993

